# Spectroscopic Detection and Evaluation of Morphologic and Biochemical Changes in Early Human Oral Carcinoma

**Markus G. Müller, Ph.D.**[1]
**Tulio A. Valdez, M.D.**[2]
**Irene Georgakoudi, Ph.D.**[1]
**Vadim Backman, Ph.D.**[1]
**Cesar Fuentes, M.D.**[3]
**Sadru Kabani, M.D.**[4]
**Nora Laver, M.D.**[5]
**Zimmern Wang, M.D.**[3]
**Charles W. Boone, M.D., Ph.D.**[1]
**Ramachandra R. Dasari, Ph.D.**[1]
**Stanley M. Shapshay, M.D.**[3]
**Michael S. Feld, Ph.D.**[1]

[1] G. R. Harrison Spectroscopy Laboratory, Massachusetts Institute of Technology, Cambridge, Massachusetts.

[2] Department of Otolaryngology, Head and Neck Surgery, Tufts University School of Medicine, New England Medical Center, Boston, Massachusetts.

[3] Department of Otolaryngology, Head and Neck Surgery, Boston University School of Medicine, Boston Medical Center, Boston, Massachusetts.

[4] Oral and Maxillofacial Pathology Department, Boston University School of Medicine, Boston, Massachusetts.

[5] Department of Pathology, Tufts University School of Medicine, New England Medical Center, Boston, Massachusetts.

This research was performed at the Massachusetts Institute of Technology Laser Biomedical Research Center and supported by National Institutes of Health Grants 5-P41-RR02594-16, and R01-CA72517-02.

Irene Georgakoudi gratefully acknowledges support from an NIH NRSA fellowship.

The authors thank George Gallagher, Raju Polavaram, Qingguo Zhang, and Josef Bille for their helpful discussions.

Drs. Fuentes, Wang, and Shapshay were formerly affiliated with the Department of Otolaryngology, Head and Neck Surgery, Tufts University School of Medicine, New England Medical Center, Boston, Massachusetts.

Address for reprints: Michael S. Feld, Ph.D., G.R. Harrison Spectroscopy Laboratory, Massachusetts Institute of Technology, 77 Massachusetts Avenue, Room 6-014, Cambridge, MA 02139; Fax: (617) 253–4513; E-mail: msfeld@mit.edu.

Received June 5, 2002; revision received August 29, 2002; accepted November 13, 2002.

**BACKGROUND.** Understanding the development and progression of head and neck squamous cell carcinoma is key in the quest for the early diagnosis and prevention of this type of malignancy. The current study correlated early biochemical and histologic changes in oral tissue with spectral features in fluorescence, reflectance, and light scattering spectra acquired in vivo to diagnose early stages of oral malignancies.

**METHODS.** A total of 91 tissue sites from 15 patients with varying degrees of malignancy (normal, dysplastic, and cancerous sites) and 8 healthy volunteers were analyzed with 3 spectroscopic techniques. Direct biochemical information regarding oral tissue native fluorophores was obtained with intrinsic fluorescence spectroscopy by fitting a linear combination of collagen and the reduced form of nicotinamide adenine dinucleotide (NADH) fluorescence spectra to the intrinsic tissue fluorescence spectra excited with 337 nanometer (nm) and 358-nm laser light. Diffuse reflectance spectroscopy was used to provide information regarding tissue absorption and structure, such as hemoglobin concentration and stroma density, by measuring the wavelength-dependent absorption and scattering coefficients. By subtracting the diffusely reflected component from the measured reflectance, light scattering spectroscopy (LSS) information resulting from single backscattering from epithelial cell nuclei was obtained. LSS provides information concerning the size distribution of cell nuclei.

**RESULTS.** These optically extracted tissue parameters provide biochemical or structural information in vivo without the need for tissue excision, and can be used to diagnose tissue abnormalities. By combining the information provided by the three techniques, a method known as trimodal spectroscopy, a sensitivity and specificity of 96% and 96%, respectively, in distinguishing cancerous/dysplastic (mild, moderate, and severe) from normal tissue was achieved. In addition, the authors were able to distinguish dysplastic from cancerous tissue with a sensitivity of 64% and a specificity of 90%.

**CONCLUSIONS.** The results of the current study demonstrated that Trimodal spectroscopy is a highly sensitive and specific technique with which to diagnose tissue abnormalities. ***Cancer* 2003;97:1681–92.** 
DOI 10.1002/cncr.11255

**KEYWORDS: Oral carcinoma, diagnosis, spectroscopy, fluorescence, reflectance, light scattering.**

Head and neck squamous cell carcinoma (HNSCC) represents a significant and growing public health problem worldwide. In the U.S. alone, approximately 30,000 new cases are diagnosed annually, and it is estimated that HNSCC results in 8000 deaths per year.[1] HNSCC has been associated with a well defined group of risk factors. Greater than 75% of patients who develop squamous cell carcinoma of the upper aerodigestive tract have a history of long-term tobacco use and heavy alcohol intake.

HNSCC is commonly preceded by dysplasia (intraepithelial neoplasia).[2] Dysplastic lesions often are found in the oral cavity in the form of erythroplakia and leukoplakia. These preinvasive neoplastic lesions carry a risk for malignant conversion of approximately 90% and 10%, respectively.[3,4] Therefore, early detection of carcinomas of the oral cavity is very important for successful treatment and improvement of the survival rate.[5] Despite advances in therapy, the inability to improve the overall survival significantly in patients with HNSCC has created strong interest in the prevention and early detection of this condition. Because the current incidence of early HNSCC is high and screening techniques are inadequate, a major challenge exists for clinicians to detect HNSCC early.[6]

The oral cavity is a complex of many tissues that differ in their histology, metabolism, and keratin content. Even though the type of epithelium is stratified squamous throughout, the mucous membrane of the oral cavity differs from region to region in the morphology of its epithelium and underlying lamina propria. The mucosa lining the oral cavity (buccal, soft palate, floor of the mouth, and inner lip) is nonkeratinized and has a loose lamina propria, whereas the specialized mucosa (dorsal tongue) and masticatory mucosa (hard palate and gingiva) have a superficial keratin layer. In addition, the masticatory mucosa has a densely packed collagen fiber network beneath the epithelium.

Detecting and distinguishing among benign, precancerous, and malignant oral lesions usually is accomplished by visual screening followed by biopsy of suspicious tissue sites. Histopathologic examination of biopsy samples is required for diagnosis. However, it often is difficult even for an experienced clinician to decide on the best area to biopsy. Field cancerous changes further complicate the diagnosis.

The presence of an identifiable high-risk population and direct access to the lesion makes the oral cavity an ideal site in which to clinically evaluate new diagnostic techniques. Techniques such as cytologic brushing may be helpful, but histologic diagnosis still is required for final diagnosis. Optical spectroscopy has the potential to detect malignant lesions earlier, before they become macroscopically visible, by probing tissue biochemistry and morphology in vivo in real time. In addition, spectroscopy may prove to be a more objective technique supplementing the clinical impression, which is known to vary among medical practitioners.

The use of endogenous and exogenous[7,8] fluorescent markers, with tumor-localizing properties, for the clinical detection of early cancer in vivo has been investigated by several researchers. However, fluorophores, absorbers, and scatterers present in tissue allow one to obtain biochemical and structural information through fluorescence, reflectance, and light scattering spectroscopy for the diagnosis of malignant and premalignant conditions, without the need to administer exogenous substances.

Fluorescence and reflectance spectroscopies already have been used for tissue assessment in various organs with promising results.[9–20] The objective of the current study was to measure biochemical and morphologic tissue parameters spectroscopically in vivo in the oral cavity and evaluate how these parameters are related to disease progression. We introduce a novel approach, trimodal spectroscopy (TMS), for analyzing fluorescence and reflectance data from oral tissue and to obtain direct morphologic and biochemical information for the diagnosis of early oral carcinoma. TMS employs three techniques: intrinsic fluorescence spectroscopy (IFS), diffuse reflectance spectroscopy (DRS), and light scattering spectroscopy (LSS). TMS has been used previously in the cervix and the esophagus, and has demonstrated promising results in detecting early malignancy. Using three independent spectroscopic techniques, TMS obtains information from different independent tissue parameters, leading to more robust diagnostic algorithms for early detection of dysplasia. This provides improved understanding of the changes in tissue morphology and biochemistry accompanying epithelial neoplasia in the oral cavity.

## MATERIAL AND METHODS

### Study Protocol

Reflectance and fluorescence spectra at multiple excitation wavelengths were collected from 53 tissue sites in 15 patients with known upper aerodigestive tract malignancies and from 38 tissue sites in 8 healthy volunteers (Table 1). The study was approved by New England Medical Center's Human Investigational Review Committee and the Massachusetts Institute of Technology's Committee on the Use of Humans as Experimental Subjects. Written informed consent was obtained from each patient and healthy volunteer enrolled in the study.

**TABLE 1**
**Site Locations and Corresponding Histopathological Diagnosis**

| | Normal | Mild dysplasia | Moderate dysplasia | Severe dysplasia | HNSCC | Inflammation | Para/ orthokeratinization |
|---|---|---|---|---|---|---|---|
| Buccal mucosa | 1 *9* | | | | 1 | | 1 |
| Floor of mouth | 5 *8* | 1 | | 4 | 5 | | |
| Soft palate | 4 | | 1 | | 3 | | |
| Ventral tongue | 1 | | 1 | 1 | | | |
| Hard palate | 1 *8* | | | 1 | | | |
| Gingiva | 3 *5* | 4 | 1 | | 3 | 2 | 2 |
| Dorsal tongue | 1 *8* | 1 | 2 | 2 | | | 1 |
| Total | 16 *38* | 6 | 5 | 8 | 12 | 2 | 4 |

HNSCC: head and neck squamous cell carcinoma; Para: parakeratotic; ortho: orthokeratotic.
Italic type indicates the number of sites from which healthy volunteer spectra were taken. No biopsies were obtained for these sites.

## Instrumentation

Fluorescence and reflectance spectra were obtained with an upgraded version of the FastEEM instrument.[21] This instrument provides 11 laser excitation wavelengths between 337 nanometers (nm) and 610 nm, which are used to acquire a fluorescence excitation-emission-matrix (EEM), and broadband white light from a xenon flash lamp (350–700 nm), which is used to obtain a diffuse reflectance spectrum. (An EEM is a three-dimensional or contour map in which fluorescence intensity is plotted as a function of excitation and emission wavelengths to fully characterize the fluorescence properties of a sample.) The excitation light is coupled into an optical fiber probe measuring approximately 1.5 mm in dimension, which is comprised of a single light delivery fiber surrounded by 6 collection fibers (fused silica, 200 $\mu$m core dimension, 0.22 numerical aperture [NA]) terminated by an optical shield (1-mm long fused silica spacer). This configuration provides a reproducible delivery-collection geometry when the probe is brought in contact with the tissue.[22] Reflected and fluorescent light emitted from tissue was collected by the probe and coupled to a spectrograph and photodiode array detector. Data acquisition and storage were computer-controlled. Calibration was performed prior to data collection.[21]

The probe was brought into gentle contact with the tissue in vivo, and fluorescence spectra at 11 excitation wavelengths and white light reflectance spectra were acquired in $<$ 1 second. To achieve a better signal-to-noise ratio (S/N), 5 sets of EEMs and reflectance were acquired at once, which took $<$ 5 seconds. The probe then was removed, leaving a temporary mark at the site at which spectra were taken, facilitating accurate biopsy sampling of the same site. In some cases, tissue markers or tattooing with ink was used to mark the tissue excitation spot for precise registration. Histology slides were prepared from the biopsies and classified by an experienced oral pathologist. After classification, the spectroscopic data was correlated with the histopathologic results.

## Methods of Analysis

Three spectroscopic techniques (IFS, DRS, and LSS) were used in combination (TMS).

### *Intrinsic fluorescence spectroscopy*

IFS is particularly important in the oral cavity because the large blood supply in this tissue can affect the fluorescence line shape and intensity. This makes it difficult to distinguish changes in tissue fluorescence, because of alterations in fluorophore concentrations, from distortions resulting from elastic scattering and hemoglobin absorption. We used a mathematic model to obtain the intrinsic tissue fluorescence spectrum and therefore quantitative biochemical information.[23,24] The intrinsic fluorescence is a linear combination of the fluorescence spectra of individual tissue biomolecules. Therefore, IFS provides direct biochemical information regarding the tissue state.

We investigated the intrinsic fluorescence of oral cavity tissue at a variety of excitation wavelengths to determine the biochemical fluorophores contributing to the tissue spectra. We anticipated that variations in the intrinsic fluorescence line shape with disease would correlate with variations in fluorophore concentration. We used multivariate curve resolution (MCR) on intrinsic fluorescence spectra of in vivo normal, dysplastic, and cancerous tissue to extract the fluorescent spectral components. The two spectral components (fluorophores) found with MCR analysis from the diseased tissues then were compared with the fluorescence from a viable cell pellet of the KB human oral squamous carcinoma cell line (predominant fluorophore the reduced form of nicotinamide

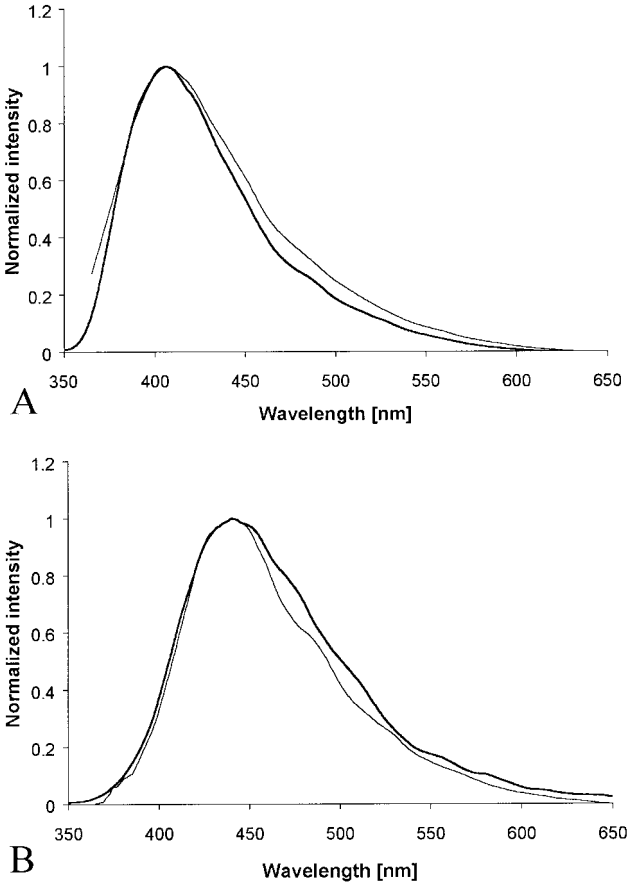


**FIGURE 1.** Intrinsic fluorescence spectra of the 2 spectral components excited at 337 nanometers (nm) and extracted with multivariate curve resolution. (A) Spectral component 1 (thin line), compared with collagen of the submucosa (thick line). (B) Spectral component 2 (thin line), compared with nicotinamide adenine dinucleotide (NADH) of a tumor cell pellet (thick line).

adenine dinucleotide [NADH]) and the submucosa of normal freshly biopsied check tissue (predominant fluorophore collagen). The two spectral components were found to be closely similar to the fluorescence of the tumor cell pellet and cheek submucosa, respectively (Fig. 1A, B), and we thus assigned the two spectral components to the fluorophores collagen and NADH.

Recovery of the intrinsic fluorescence and knowledge of the fluorescent components allow quantitative biochemical analysis of the tissue. A linear combination of NADH and collagen spectral components from the MCR algorithm were fitted to the intrinsic tissue fluorescence spectra for 337 nm and 358 nm excitation, respectively, from patients and healthy volunteers. These excitation wavelengths were chosen because the spectral line shapes of NADH and collagen at these wavelengths are appreciably different, and the fluorescence intensity of NADH (for which the excitation spectrum approaches 0 for wavelengths $>$ 400 nm) is strong enough to be detectable. To investigate the natural variations in the intrinsic fluorescence spectra from different normal tissue sites in the oral cavity, spectra from eight healthy volunteers were analyzed.

### *Diffuse reflectance spectroscopy*

DFS also has shown promise as a diagnostic tool. Diffusely reflected white light enters the tissue and scatters multiple times before it is collected at the tissue surface. Spectral analysis of the reemerging light, based on diffusion theory, provides biochemical information from the absorption and structural information because of scattering.[9,18,19,25] Diffuse reflectance spectra in the range of 350–700 nm were analyzed using a model based on light diffusion theory to extract the absorption and reduced scattering coefficients of tissue.[9] In some cases in which the fit over the entire wavelength range was quite poor (because of the large hemoglobin absorption of approximately 420 nm and the layered structure of the tissue), fits of the reflectance spectrum were restricted from 500 nm to 700 nm. Hemoglobin was found to be the dominant absorber for these tissues in the visible range of the spectrum. Scattering was approximated by the Mie theory. The scattering properties of diffusely reflected light are determined mainly by the collagen fibers of the underlying stromal layer.[26] Thus, DRS provides information regarding the morphology and biochemistry of the stroma. By using the diffusion model[9] to fit the experimental data, the absorption ($\mu_a$) and reduced scattering coefficient spectra ($\mu_s'$) were obtained as functions of wavelength.

### *Light scattering spectroscopy*

LSS studies white light backscattered from cell nuclei, which can be approximated by spheres of appropriate dimension and refractive index.[27] According to the Mie theory, the light from these scatterers contains an oscillatory component in wavelength, the frequency and amplitude of which are proportional to the dimension and density, respectively. Measured size (nuclear enlargement) and density (crowding) are key parameters used by pathologists to diagnose dysplasia. The diagnostic potential of LSS has been demonstrated in the esophagus, bladder, oral cavity, colon,[10] and cervix.[19] The LSS spectrum was extracted from the reflectance spectrum by subtracting the diffuse component obtained from the model fit.[9] In some cases, we had to modify this model to obtain good fits by superposing two modeled reflectance spectra. After subtracting the model fit from the experimentally ob-

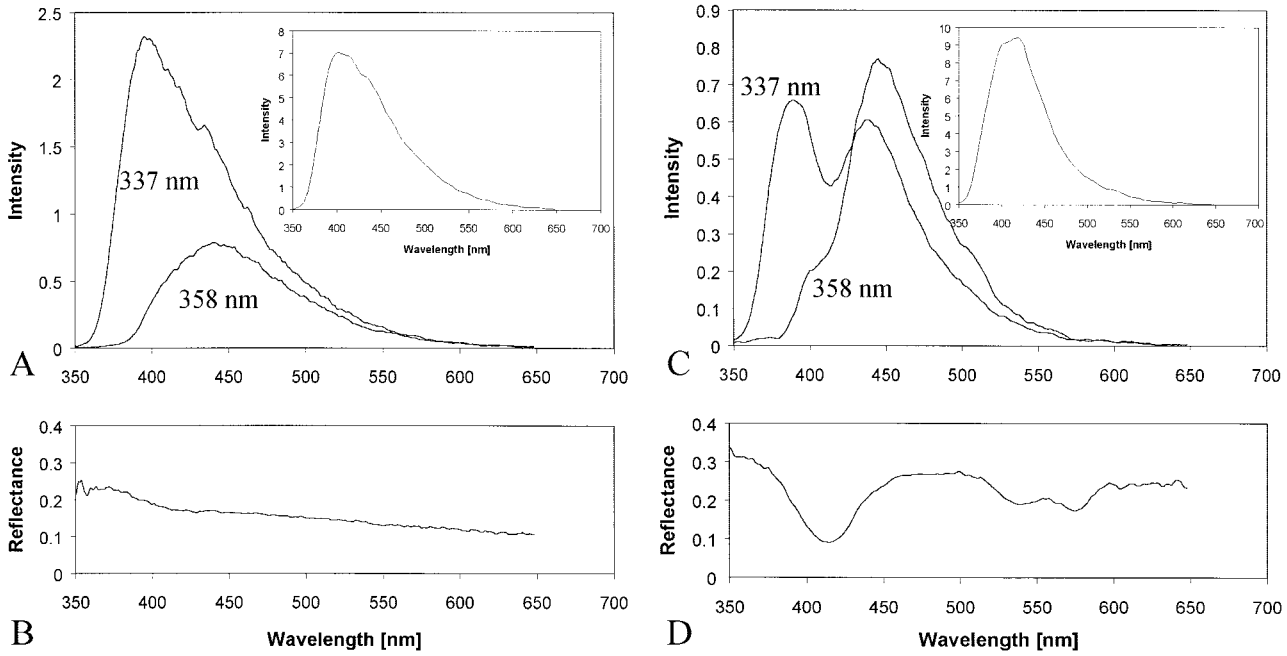


**FIGURE 2.** Tissue fluorescence spectra measured at two sites (Panels A, C), each excited at 337 nanometers (nm) and 358 nm, respectively, and corresponding tissue reflectance spectra at those sites (Panels B, D). The large differences in line shape between Panels A and C are apparent especially at 337-nm excitation, and are for the most part the result of hemoglobin variations, which also can be observed in the 2 reflectance spectra. For comparison, the *insets* show the 337-nm excited intrinsic fluorescence.

tained reflectance, the size distribution of nuclei was extracted.[27]

### Statistical Analysis

To assess the diagnostic potential of IFS, DRS, and LSS, we used a statistical technique called logistic regression, which correlates the results of each spectroscopic technique with histopathology. To establish the ability of spectroscopy to predict the presence of disease (malignancy, dysplasia) and nondisease (normal) accurately, we employed a cross-validation scheme in which one data point was removed, the remaining data points were used to develop a classification scheme, and the result was applied to the omitted data point.[28] This process was repeated until all data points were evaluated. The same scheme was used in the classification of dysplasia versus malignancy. In the current study, all dysplastic and cancerous sites previously falling in the wrong category (normal) were labeled as misclassified. The spectra from six benign tissues sites diagnosed as hyperplasia (one site), hyperkeratosis (two sites), parakeratosis (one site), and inflammation only (two sites) were not incorporated in the statistical analysis because of the small size of these categories.

#### *Trimodal spectroscopy*

The three techniques were combined to form a consensus TMS diagnosis in which the combined diagnosis of each site was obtained as the diagnosis for which the results of at least two of the three techniques agreed. The advantage of TMS is that the use of several diagnostic parameters for diagnosis can potentially increase the prediction accuracy significantly.

## RESULTS

#### *Intrinsic fluorescence spectroscopy*

Figure 2 shows measured reflectance and fluorescence spectra at 337 nm and 358 nm excitation, respectively, taken in 2 samples. Strong variations in both reflectance and fluorescence can be noted. There are two types of variations in the fluorescence: changes in the fluorescent properties of the tissue and distortions by absorption and scattering. The latter variations, predominantly the result of hemoglobin, can be removed by extracting the intrinsic fluorescence, which results in fluorescence variations that are the result of changes in fluorophore concentrations only. Therefore, a line shape shift in the intrinsic fluorescence for cancerous tissue can be attributed to biochemical and/or morphologic changes.[24]

The intrinsic fluorescence spectra from normal

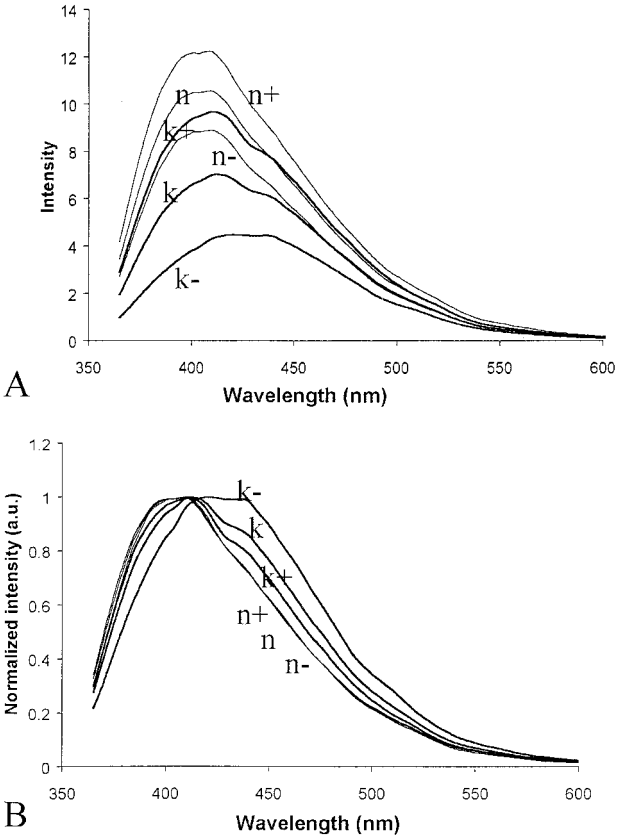


**FIGURE 3.** Mean intrinsic fluorescence spectra with standard deviations (±) from normal tissue with keratinized epithelium (k) and nonkeratinized epithelium (n). (A) Unnormalized and (B) Normalized spectra. Excitation is at 337 nanometers (nm). Note the differences in intensity, line shape, and standard deviation. a.u.: arbitrary units.

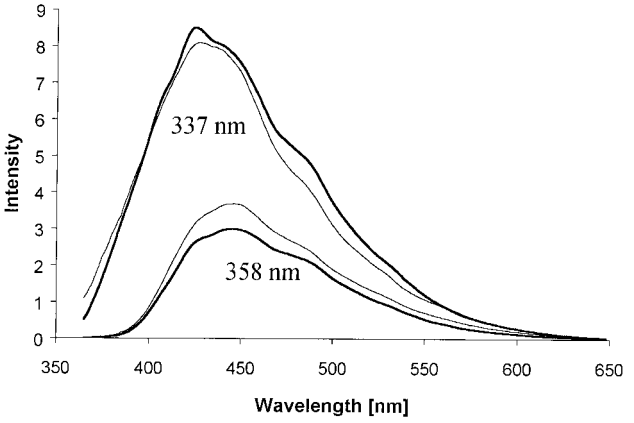


**FIGURE 4.** Intrinsic fluorescence spectra of a cancerous tissue site at two excitation wavelengths (thick line), fit to a linear combination of the two spectral components (thin line). Note that the model recovers the relative fluorescence intensities, as well as the spectral line shapes. nm: nanometers.

tissue sites were divided into two classes: keratinized and nonkeratinized. We found that normal tissue with keratinized epithelium, such as specialized and masticatory mucosa, have intrinsic fluorescence spectra that are somewhat lower in intensity (Fig. 3A) and are shifted to the red region of the spectrum compared with spectra from mucosa lining of the oral cavity (Fig. 3B). Because of these variations in the normal sites, we divided our data set into these two basic categories. Subsequent data analysis found that this procedure resulted in the best separation between normal and diseased tissue sites.

We found the diagnostically significant information in the intrinsic fluorescence spectra to lie in the emission wavelength range of 350–600 nm. As discussed earlier, at these wavelengths the intrinsic fluorescence of oral cavity tissue is comprised of the two spectral components, collagen and NADH. From the variations in the intrinsic fluorescence spectra with progression of disease, we further concluded that tissue has varying amounts of these fluorophores whereby NADH increases and collagen decreases with disease. A typical fit of these spectral components to a cancerous tissue site is shown in Figure 4.

Figure 5 is a binary plot of the relative contributions from NADH and collagen spectral components. As can be observed, all three tissue types (normal, dysplastic, and cancerous) are well separated (Table 2, first row, panels A, B).

### *Diffuse reflectance spectroscopy*

A typical diffuse reflectance fit using the model by Zonios et al.[9] to the experimentally obtained reflectance is shown in Figure 6A. The fit provides the absorption, $\mu_a(\lambda)$, and reduced scattering coefficient spectra, $\mu_s'(\lambda)$. An absorption coefficient comprised of only hemoglobin gave a good fit to the reflectance, indicating that hemoglobin is the only significant absorber. The absorption coefficient demonstrated large variations in hemoglobin concentration, which were found to be uncorrelated with disease. To characterize the overall intensity and slope of the reduced scattering coefficient ($\mu_s'$), a linear fit was performed (Fig. 6B). Analysis of the reflectance data from healthy volunteers demonstrated a general trend toward higher scattering coefficients for keratinized compared with nonkeratinized epithelium, which is expected because of the previously discussed differences in morphology. Therefore, we separated the data into two basic categories, as was done for the intrinsic fluorescence. Figures 6C and 6D show binary plots with the intercepts at $\lambda = 0$ nm and the slopes of the lines fitted to the extracted $\mu_s'(\lambda)$. The trend toward smaller and flatter values of $\mu_s'(\lambda)$ with increasing extent of dysplasia and

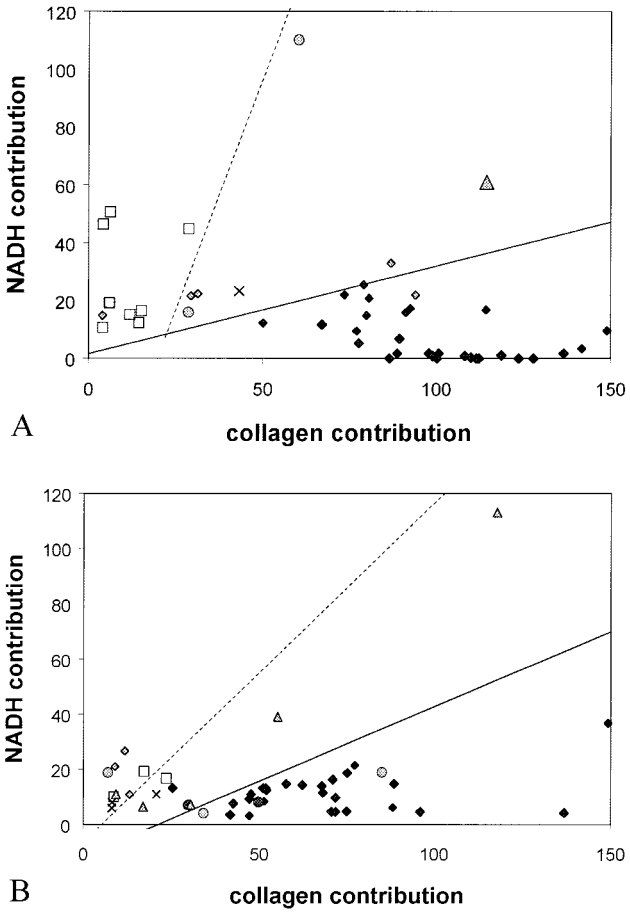


**FIGURE 5.** Binary decision plots, demonstrating the collagen and the reduced form of nicotinamide adenine dinucleotide (NADH) contributions to the intrinsic fluorescence tissue spectra at 337- nanometers (nm) and 358 nm excitation. (A) Nonkeratinized, and (B) keratinized epithelium. Note that the collagen contribution decreases and the NADH contribution increases with progression toward malignancy. The solid line separates the normal from the abnormal tissue and the dotted line separates dysplasic from cancerous tissue. Darkly shaded diamond: normal; darkly shaded triangle: mild dysplasia; shaded circle: moderate dysplasia; lightly shaded diamond: severe dysplasia; open square: cancerous tissue; solid circle: inflammation; X: hyperkeratosis.

malignancy can be used to make diagnostic decisions (Table 2, second row, Panels A, B).

### *Light scattering spectroscopy*

Light scattering spectra can be extracted from tissue reflectance spectra by subtracting the modeled diffuse reflectance fit from the data. The data quality and fits of the diffuse reflectance model were not always good enough over the entire wavelength range (350–700 nm) to permit extraction of LSS spectra. (The larger the wavelengths range, the more oscillations in the LSS spectrum, thereby improving the accuracy of the fit). In some cases the data fits could be improved by modifying the diffuse reflectance model as discussed earlier, thus enabling LSS spectra extraction. Because LSS analysis requires high quality spectra with good S/N, some data points (spectra) had to be omitted from the data analysis. Because LSS provides only information regarding epithelial nuclei, separation of the data set into two classes was not necessary. The results from the analyzed spectra (Fig. 7) demonstrate an enlargement of epithelial cell nuclei and broadening in the nuclear size distribution with disease (Table 2, third row, Panels A, B).

### Statistical Analysis

The logistic regression lines in Figures 5–7 demonstrate good separation between normal and abnormal (solid line) and dysplasia and carcinoma sites (dotted line). The lines demarcate the area for which a certain diagnosis is expected when certain optical parameters are obtained. The spread in the data points is because of biologic variations and possible sampling errors. Points that were misclassified in the first classification step (normal vs. abnormal) also were counted as misclassified in the second step (dysplasia vs. carcinoma).

### *Trimodal spectroscopy*

Combining the three spectroscopic techniques provided increased accuracy to characterize normal and abnormal tissues, and also improved our ability to differentiate between cancerous and dysplastic tissue. For TMS analysis, we used a consensus diagnosis in which at least two of the three techniques provided the same classification as the histopathologic diagnosis. The last row of Table 2 indicates that TMS has a higher sensitivity and specificity than was achieved with any one of the other techniques alone. This combination enabled us to diagnose malignant/precancerous tissues with a sensitivity of 96% and a specificity of 96% and a positive and negative predictive value of 0.93 and 0.98, respectively (only 1 abnormal and 2 normal sites were misclassified). In addition, we distinguished cancerous from dysplastic tissue with a sensitivity of 64% and a specificity of 90% (with positive and negative predictive values of 0.9 and 0.64, respectively).

## DISCUSSION

Currently the standard for dysplasia and carcinoma detection in the oral cavity is visual screening, biopsy, and histopathologic evaluation. Tissue structural and biochemical changes during carcinoma development include several features that can be measured optically, including hyperproliferation and nuclear crowding of basal cells. The epithelium frequently demonstrates thickening, loss of cell stratification, and

**TABLE 2**
**Spectroscopic Versus Pathologic Classification**

**A. Normal and abnormal tissue**

| | Nonkeratinized | | Keratinized | | Total | |
|---|---|---|---|---|---|---|
| | Abnormal Spectr/histopath | Normal Spectr/histopath | Abnormal Spectr/histopath | Normal Spectr/histopath | Abnormal Spectr/histopath | Normal Spectr/histopath |
| IFS | 16/17 | 27/28 | 12/14 | 25/26 | 28/31 | 52/54 |
| DRS | 15/17 | 19/28 | 9/14 | 21/26 | 23/31 | 40/54 |
| LSS | 13/14 | 17/17 | 9/10 | 16/17 | 22/24 | 33/34 |
| TMS | 16/16 | 22/23 | 11/12 | 22/23 | 27/28 | 44/46 |

**B. Dysplastic versus cancerous tissue**

| | Nonkeratinized | | Keratinized | | Total | |
|---|---|---|---|---|---|---|
| | Dysplastic spectr/histopath | Carcinoma spectr/histopath | Dysplastic spectr/histopath | Carcinoma spectr/histopath | Dysplastic spectr/histopath | Carcinoma spectr/histopath |
| IFS | 5/8 | 8/9 | 5/11 | 2/3 | 10/19 | 10/12 |
| DRS | 2/8 | 6/9 | 5/11 | 2/3 | 7/19 | 8/12 |
| LSS | 3/6 | 4/8 | 6/8 | 1/2 | 9/14 | 5/10 |
| TMS | 3/6 | 7/8 | 6/8 | 2/2 | 9/14 | 9/10 |

Spectr/histopath: Optical spectroscopy/histopathologic examination; IFS: intrinsic fluorescence spectroscopy; DRS: diffuse reflectance spectroscopy; LSS: light scattering spectroscopy; TMS: trimodal spectroscopy.

enlargement of epithelial cell nuclei.[2] The development of dysplasia and carcinoma commonly is associated with inflammatory changes, including neovascularization.[29] The lamina propria undergoes reorganization and matrix metalloproteinases (MMPs) degrade parts of the basement membrane and underlying collagen network, facilitating tumor cell invasion and ultimately metastatic dissemination via the lymphatic and vascular systems.[30]

Several investigators have conducted clinical studies to examine the potential of fluorescence to diagnose dysplasia and carcinoma in the oral cavity using endogenous or exogenous fluorophores. Markers such as 5-aminolevulinic acid (5-ALA)-induced protoporphyrin IX (PPIX) or hematoporphyrin derivative (HPD) may be administered systemically or topically. These fluorescent substances appear to accumulate to a greater extent in cancerous tissue compared with in normal tissue. HPD and PPIX are reported to have a low specificity for detecting carcinoma[7] and are not very sensitive for detecting early neoplastic lesions. Red porphyrin fluorescence also can be observed, mostly in HNSCC, without the use of exogenous dyes.[31]

In the past, endogenous porphyrin fluorescence excited at 410 nm was used to detect abnormal tissue sites in the oral cavity.[11,14,32,33] This method may achieve high sensitivity to detect cancerous lesions, but its specificity tends to be low. In the current study, we observed red fluorescence not only in HNSCC sites but also in some oral cavity sites of healthy volunteers. This, among other effects, might be because of bacterial colonization in the oral cavity, which also produces PPIX.[34] Heintzelman et al.[35] studied the fluorescence from several excitation wavelengths and used the ratio between 350–400 nm excitation at 472 nm emission as an optimal diagnostic algorithm for detecting malignant abnormalities of the oral cavity with fluorescence spectroscopy. They and others[8,33,36] achieved good results, especially for ultraviolet excitation, using diagnostic decision algorithms based on empiric observations or principal component analysis. However, often, no statistical validation was used on the data sets. Use of these algorithms to acquire insight into biologic changes can be misleading because variations in hemoglobin concentration and tissue structure also can alter the fluorescence, leading to interpatient and same-patient variations.[32,33] The results of the current study demonstrate that by using the intrinsic fluorescence of tissue, the effect of variations in absorber (e.g., hemoglobin) concentration and therefore in fluorescence line shape and intensity can be removed (*insets,* Fig. 2). This allowed us to analyze fundamental underlying changes in the fluorescence spectra produced by tissue changes (biochemical composition) alone, whereas previous studies simply attempted to correlate spectral features with general tumor development.

Two spectral components of the oral cavity, NADH and collagen, allowed us to extract cellular

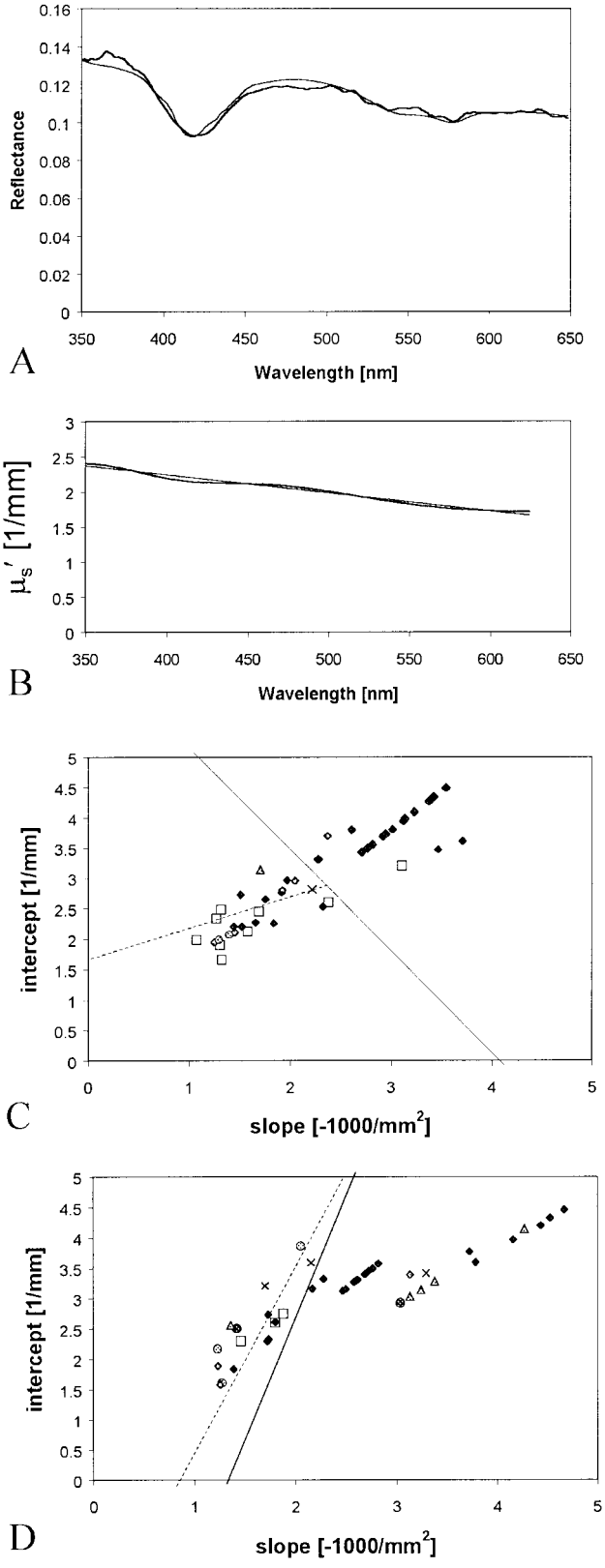


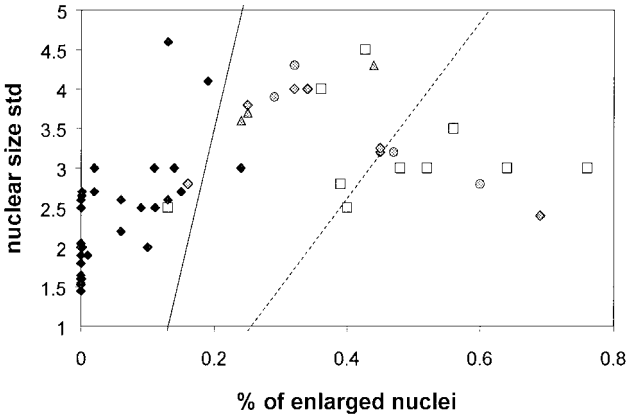


**FIGURE 7.** Binary decision plot showing the standard deviation (std) of the nuclei size distribution plotted as a function of percentage of enlarged nuclei (dimension $>$ 10 $\mu$m). The solid line separates normal from abnormal tissue and the dotted line separates dysplasic from cancerous tissue. Darkly shaded diamond: normal; shaded triangle: mild dysplasia; shaded circle: moderate dysplasia; lightly shaded diamond: severe dysplasia; open square: cancerous tissue; solid circle: inflammation, X: hyperkeratosis.

fluorescence because of cell number and metabolic activity and stromal fluorescence in vivo, respectively. The line shape shift to the red and the smaller overall fluorescence intensity for keratinized tissues noted in Figure 3 most likely is because of the keratin layer on the surface of the epithelium. Compared with nonkeratinized tissue, the keratin layer scatters some of the incoming excitation light and reduces the depth of penetration. This results in an NADH contribution that is relatively higher than that of collagen. Keratin fluorescence also might contribute to the spectrum; however, a distinct spectrum for this biochemical was not required to describe the intrinsic tissue fluorescence accurately.

The increased cell and metabolic activity associated with the progression of neoplastic disease leads to an increase in NADH fluorescence. In addition, because of the thickening of the epithelium, less exci-

**FIGURE 6.** (A) Reflectance spectrum of normal oral mucosa (thick line) with model fit (thin line). (B) Linear fit (thin line) to the reduced scattering coefficient (thick line) extracted from Panel A. (C, D) Slopes and intercepts of linear fits to the reduced scattering coefficients of tissue reflectance spectra. (C) Nonkeratinized and (D) keratinized epithelium. The solid line separates normal from abnormal tissue and the dotted line separates dysplasic from cancerous tissue. nm: nanometers; darkly shaded diamond: normal; shaded triangle: mild dysplasia; shaded circle: moderate dysplasia; lightly shaded diamond: severe dysplasia; open square: cancerous tissue; solid circle: inflammation; X: hyperkeratosis.

tation light can reach the underlying collagen network. It also has been shown that collagenase enzymes responsible for the degradation of collagen usually are present in tissue areas undergoing significant architectural changes.[37] Differences in the levels and expression of MMPs were found between normal squamous oral tissue and HNSCC.[38] These are believed to be the reasons why NADH and collagen contributions to the tissue fluorescence spectrum changed markedly with progression of disease, which also was observed previously in Barrett esophagus and the cervix.[18,19] Some of the cancerous and dysplastic specimens demonstrated parakeratotic and orthokeratotic features (clinical impression: leukoplakia) on the histology slide and still were classified correctly by spectroscopy. Future studies will be needed to establish how the thickness of the keratin layer affects our capability to detect dysplastic changes beneath it. The layered structure of squamous mucosa did not appear to affect the fluorescence line shape as much as the reflectance spectra, which might be because of the much larger bandwidth of the reflectance.

The spectral changes produced by structural and biochemical changes in the epithelium and the subepithelial collagen network also are noted in the reflectance spectra. Small differences were discovered between keratinized and nonkeratinized tissue sites, and even between buccal mucosa and the floor of the mouth, in which the latter was found to exhibit slightly greater scattering. Decreased scattering of buccal tissue may be the result of the increased thickness of its epithelium, making it harder for light to reach the collagen fibers (major scatterers) in the lamina propria and underlying stroma. However, in the masticatory tissue, the increased scattering might be the result of the surface keratin layer and the dense collagen fiber network in the lamina propria. This keratin layer may even increase further and develop into hyperkeratosis (clinical impression: leukoplakia). The hyperkeratotic lesion appears white to the examining physician because of the increased scattering by the thickened keratin layer hindering the light from reaching the deeper vascular layers. Despite all these morphologic and biochemical variations, we still were able to observe scattering changes resulting from dysplasia and carcinoma. The decrease in the scattering coefficient may be explained by thickening of the epithelium and a slow destruction of collagen cross-links by MMPs.

Microscopic tissue changes in the epithelium could be detected with LSS. Enlargement of epithelial cell nuclei and the increase in the standard deviation of the nuclear size distribution are well established biomarkers of dysplastic cells and are commonly used by pathologists in making diagnostic decisions. The enlargement and variations in cell nuclear size are because of the increase in the mean and variance of nuclear DNA content, produced by errors in the mitotic process that lead to aneuploidy (additional fragments of often broken copies of gene segments in the nucleus).[2] This is consistent with the finding of Sudbo et al.[39] that dysplastic lesions (clinically diagnosed as leukoplakia) with aneuploidy have a high probability (84%) of developing into HNSCC. Previously, we found that nuclear crowding also is a good parameter for detecting dysplastic lesions in the oral cavity.[10] We observed the same trend in this data set. However, we found that nuclear size standard deviation is a better diagnostic parameter than crowding.

Because LSS is sensitive to singly scattered light, the information obtained is limited to the epithelium, which complements the information from deeper tissue layers obtained with DRS. The direct backscattering detection geometry makes this technique more sensitive to structures of the size of cell nuclei, and interference from cell scattering can be neglected. Very good results were obtained for LSS. However, because of the small LSS signal (2–5% of the overall reflectance signal), good data quality and agreement with the diffuse reflectance model fit is required for a reliable LSS analysis, which could not be achieved in all cases in the current study.

The utilization of all three techniques for tissue characterization provides several types of information: biochemical, stromal scattering/absorption, and size distribution of the epithelial nuclei. By combining the biochemical and morphologic information of tissues extracted from IFS, DRS, and LSS, we achieve a more sensitive and specific diagnosis. The lower sensitivity and specificity for distinguishing between dysplasia and malignancy may be a reflection of the increased structural and biochemical variability of tumor tissue in general. Necrotic tumors, for example, may be comprised of cells that are terminally apoptotic or dead and disintegrating. In addition, some dysplasia spectra were obtained at the margin of the tumor so that registration of the 1-mm spectroscopically probed tissue spot and the 2–3-mm biopsy might have not been optimal. We also noted that the histopathology results, which were used as the standard, are themselves subject to strong intraexaminer and interexaminer variations.[40] However, distinguishing carcinoma from normal tissue appeared to present no problems, and resulted in correct classification of all tissue sites. Because some of the LSS data points could not be analyzed, we could not obtain a consensus diagnosis (TMS) for all data points and had to exclude those for which the IFS diagnosis did not agree with the DRS diagnosis. Several published studies have reported a

good separation between cancerous and normal tissue but to our knowledge none have attempted to distinguish between cancerous and dysplastic tissue.[11,16,36] The good results we have obtained with our spectroscopic techniques suggest that TMS may be used as a guide to biopsy, thereby enhancing the physician's ability to detect lesions at an early stage.

The current study used modeling of fluorescence and reflectance spectra of the oral cavity to extract quantitative biochemical and morphologic features associated with carcinoma progression. Thus, complementary structural and biochemical information was extracted from a macroscopic tissue sample of approximately 1 $mm^3$ in dimension. Some of these morphologic features are customarily employed qualitatively by pathologists in making their diagnoses. Thus, we could create a novel tissue classification scheme built on modeling spectra to derive the underlying causal features in malignant tissue progression.

## Conclusions

The rich source of information and diagnostic potential provided by noninvasive spectroscopic techniques allows us to understand more fully the changes that take place during the onset and progression of neoplasia. The results of the current study demonstrated that NADH-collagen changes have excellent diagnostic potential. Tissue hemoglobin concentration and changes in stromal morphology are extracted from the diffuse reflectance. Additional morphologic information regarding epithelial cell nuclei is contained in the light scattering spectra. All tissue biochemical and structural information in the current study was obtained in vivo without the use of exogenous dyes, and without the introduction of artifacts due to tissue removal and processing. Finally, use of the 3 spectroscopic techniques together resulted in a sensitivity of 96% and a specificity of 96% in distinguishing normal from abnormal tissue and a sensitivity of 64% and a specificity of 90% in distinguishing cancerous from dysplastic tissue.

The results of the current study advances our understanding of the progression from normal to dysplastic to cancerous tissue. Currently, we are working on extending our analysis to real time, which will provide biopsy guidance to the physician during early screening for malignancy and will allow for the detection of tumor margins in the operating room.

## REFERENCES


1. Wingo PA, Tong T, Bolden S. Cancer statistics. *CA Cancer J Clin.* 1995;45:8–30.
2. Boone CW, Bacus JW, Bacus JV, Steele VE, Kelloff GJ. Properties of intraepithelial neoplasia relevant to cancer chemoprevention and to the development of surrogate end points for clinical trials. *Proc Soc Exp Biol Med.* 1997;216: 151–165.
3. Shafer WG, Waldron CA. Erythroplakia of the oral cavity. *Cancer.* 1975;36:1021–1028.
4. Suarez P, Batsakis JG, el-Naggar AK. Leukoplakia: still a gallimaufry or is progress being made?-a review. *Adv Anat Pathol.* 1998;5:137–155.
5. Silverman S Jr. Oral cancer, 4th edition. London: BC Decker Inc., 1998:70–75.
6. Bouquot JE, Kurland LT, Weiland LH. Carcinoma in situ of the upper aerodigestive tract. Incidence, time trends, and follow-up in Rochester, Minnesota, 1935-1984. *Cancer.* 1988;61:1691–1698.
7. Leunig A, Betz CS, Mehlmann M, et al. Detection of squamous cell carcinoma of the oral cavity by imaging 5-aminolevulinic acid-induced protoporphyrin IX fluorescence. *Laryngoscope.* 2000;110:78–83.
8. Eker C, Rydell R, Svanberg K, Andersson-Engels S. Multivariate analysis of laryngeal fluorescence spectra recorded in vivo. *Lasers Surg Med.* 2001;28:259–266.
9. Zonios G, Perelman LT, Backman V, et al. Diffuse reflectance spectroscopy of human adenomatous colon polyps in vivo. *Appl Opt.* 1999;38:6628–6637.
10. Backman V, Wallace M, Perelman LT, et al. Detection of preinvasive cancer cells. *Nature.* 2000;406:35–36.
11. Betz CS, Mehlmann M, Rick K, et al. Autofluorescence imaging and spectroscopy of normal and malignant mucosa in patients with head and neck cancer. *Lasers Surg Med.* 1999;25:323–334.
12. Anidjar M, Cussenot O, Avrillier S, et al. Ultraviolet laser-induced autofluorescence distinction between malignant and normal urothelial cells and tissues. *J Biomed Opt.* 1996;1:335–341.
13. Alfano RR, Tata DB, Cordero J, et al. Laser induced fluorescence spectroscopy from native cancerous and normal tissue. *IEEE J Sel Top Quant Electron.* 1984;20:1507–1511.
14. Dhingra JK, Zhang X, McMillan K, et al. Diagnosis of head and neck precancerous lesions in an animal model using fluorescence spectroscopy. *Laryngoscope.* 1998;108:471–475.
15. Gillenwater A, Jacob R, Richards-Kortum R. Fluorescence spectroscopy: a technique with potential to improve the early detection of aerodigestive tract neoplasia. In: Snyderman CH, editor. Head & neck: aerodigestive tract neoplasia. New York: John Wiley & Sons, Inc., 1998;556–562.
16. Schantz SP, Koli V, Savage HE, et al. In vivo native fluorescence and histological characteristics of head and neck cancer. *Clin Cancer Res.* 1998;4:1177–1182.
17. Schomacker KT, Frisoli JK, Compton CC, et al. Ultraviolet laser-induced fluorescence of colonic tissue basic biology and diagnostic potential. *Lasers Surg Med.* 1992,12:63–78.
18. Georgakoudi I, Jacobson BC, Van Dam J, et al. Fluorescence, reflectance and light scattering spectroscopy for evaluating dysplasia in patients with Barrett's esophagus. *Gastroenterology.* 2001;120:1620–1629.
19. Georgakoudi I, Sheets EE, Müller MG, et al. Tri-modal spectroscopy as a tool for detection and biochemical/morphological characterization of cervical precancers in vivo. *Am J Obstet Gynecol.* 2002;186:374–382.
20. Richards-Kortum R, Sevick-Muraca E. Quantitative optical spectroscopy for tissue diagnosis. *Annu Rev Phys Chem.* 1996;47:555–606.

21. Zangaro RA, Silveira L Jr. Manoharan R, et al. Rapid multiexcitation fluorescence spectroscopy system for in vivo tissue diagnosis. *Appl Opt.* 1996;35:5211–5219.
22. Cothren RM, Hayes GB, Kramer JR, et al. A multifiber catheter with an optical shield for laser angiosurgery. *Lasers Life Sci.* 1986;1:1–12.
23. Zhang Q, Müller MG, Wu J, Feld MS. Turbidity-free fluorescence spectroscopy of biological tissue. *Opt Lett.* 2000; 25:1451–1453.
24. Müller MG, Georgakoudi I, Zhang Q, Wu J, Feld MS. Fluorescence in turbid media: disentangling effects of scattering and absorption. *Appl Opt.* 2001;40:4633–4646.
25. Mourant JR, Bigio IJ, Boyer J, Conn RL, Johnson T, Shimada T. Spectroscopic diagnosis of bladder cancer elastic light scattering. *Lasers Surg Med.* 1995;17:350–357.
26. Saidi I, Jacques S, Tittel F. Mie and Rayleigh modeling of visible-light scattering in neonatal skin. *Appl Opt.* 1995;34: 7410–7418.
27. Perelman LT, Backman V, Wallace M, et al. Observation of periodic fine structure in reflectance from biological tissue: a new technique for measuring nuclear size distribution. *Phys Rev Lett.* 1998;80:627–630.
28. Schumacher M, Hollander N, Sauerbrei W. Resampling and cross-validation techniques: a tool to reduce bias caused by model building? *Stat Med.* 1997;16:2813–2827.
29. Lee AH, Happerfield LC, Bobrow LG, Millis RR. Angiogenesis and inflammation in invasive carcinoma of the breast. *J Clin Pathol.* 1997;50:669–673.
30. Bodey B, Bodey BJ, Siegel SE, Kaiser HE. Matrix metalloproteinase expression in malignant melanomas: tumor-extracellular matrix interactions in invasion and metastasis. *In Vivo.* 2001;15:57–64.
31. Inaguma M, Hashimoto K. Porphyrin-like fluorescence in oral cancer. *Cancer.* 1999;86:2201–2211.
32. Dhingra JK, Perrault DF, McMillan K, et al. Early diagnosis of upper aerodigestive tract cancer by autofluorescence. *Arch Otolaryngol Head Neck Surg.* 1996;122:1181–1186.
33. Gillenwater A, Jacob R, Ganeshappa R, et al. Noninvasive diagnosis of oral neoplasia based on fluorescence spectroscopy and native tissue autofluorescence. *Arch Otolaryngol Head Neck Surg.* 1998;124:1251–1258.
34. Ghadially FN, Neish WJP, Dawkins HC. Mechanisms involved in the production of red fluorescence of human experimental tumors. *J Pathol Bact.* 1963;83:77–92.
35. Heintzelman DL, Utzinger U, Fuchs H, et al. Optimal excitation wavelengths for in vivo detection of oral neoplasia using fluorescence spectroscopy. *Photochem Photobiol.* 2000;72:103–113.
36. Majumder SK, Gupta PK, Uppal A. Autofluorescence spectroscopy of tissues from human oral cavity for discriminating malignant from normal. *Lasers Life Sci.* 1999; 8:211–227.
37. Ellis DL, Yannas IV. Recent advances in tissue synthesis in vivo by use of collagen-glycosaminoglycan copolymers. *Biomaterials.* 1996;17:291–299.
38. Sutinen M, Kainulainen T, Hurskainen T, et al. Expression of matrix metalloproteinases (MMP-1 and -2) and their inhibitors (TIMP-1, -2 and -3) in oral lichen planus, dysplasia, squamous cell carcinoma and lymph node metastasis. *Br J Cancer.* 1998;77:2239–2245.
39. Sudbo J, Kildal W, Risberg B, Koppang H, Danielsen H, Reith A. DNA content as a prognostic marker in patients with oral leukoplakia. *N Engl J Med.* 2001;344:1270–1278.
40. Abbey LM, Kaugars GE, Gunsolley JC, et al. Intraexaminer and interexaminer reliability in the diagnosis of oral epithelial dysplasia. *Oral Surg Oral Med Oral Pathol Oral Radiol Endod.* 1995;80:188–191.